Nanostructural interface and strength of polymer composite scaffolds applied to intervertebral bone

Bankole I. Oladapo [a,b,*], Sikiru O. Ismail[c], Aderogba V. Adebiyi[a,d], Francis T.Omigbodun[e], Mattew A.Olawumi[b], David B.Olawade[f],

[a]*Engineering Department, Heart of Worcestershire College, Worcester, UK*

[b]*School of Engineering and Sustainable Development, De Montfort University, United Kingdom*

[c]*School of Physics, Engineering and Computer Science, University of Hertfordshire, United Kingdom*

[d]*Faculty of Engineering, Environment and Computing, Coventry University, UK*

[e]*Wolfson School of Mechanical, Electrical and Manufacturing Engineering, Loughborough University, UK*

[f]*Department of Environmental Health Sciences, University of Ibadan, Nigeria*

* Corresponding author: B.I. Oladapo, E-mail: E8217@howcollege.ac.uk

Abstract

The pores of bone tissue that play an important part in bone regeneration can emulate the areas of nanoparticles from porous scaffolds. This work evaluated a novel designed and developed nanostructure surface of polyetheretherketone-reduced graphene oxide, calcium hydroxyapatite (PEEK-rGO-cHAp) composite scaffolds of four different lattice structures. The scaffolds were fabricated through fused deposition modelling (FDM), as rGO-cHAp composite was coated on PEEK. The composite scaffolds' mechanical strength and surface microstructure were studied, using different nanostructure methods of unit cell homogenisation and tensile test. The homogenisation method for the four lattice structures was designed and analysed to mimic spine bone structure. A new approach was introduced to homogenise the mechanical characteristics of a periodical lattice of 3D printing structures based on a semi-rigid frame unit cell. They were taking into consideration the impact of geometric approximation errors and joint tightening. A typical frame element with semi-rigid is integrated to assess combined stiffening effects in a discrete homogenisation process. The analysis was performed by considering the fundamental unit cell as a scaffold that defined the periodic pattern. Also, this study created an avenue to examine and improve the interfacial bonding between PEEK and rGO-cHAp scaffolds for biocompatibility and degradability, using surface functionalisation techniques. This work aimed to compare the manufacturing processes in an intervertebral spacer model and its lattice structure, present the characteristics of the PEEK biomaterial and some parameters used for its processing. In addition to its manufacturing part, a brief theory on the anatomy of the spine region was also presented. The object of the study was applied, which in this case was the cervical region, with a surgical approach through an anterior method to establish its practical applications and benefits in tissue engineering.

Keywords: Spine implant; Polyetheretherketone; Homogenisation; Lattice structures; PEEK-rGo-cHAp;

1. Introduction

Due to diseases related to life and other congenital problems, the demand for spinal implants has increased dramatically in recent years. His condition is aggravated by the fact that the individual is born with illness and time. One alternative for alleviating or resolving the effects of these diseases is the use of cross-bridge spacers in

the area to be treated [1-3]. This case promotes bone arthrodesis - a fusion of vertebrae, stabilisation of the spinal cord, and primarily pain relief. A polymer known as polyetheretherketone (PEEK) may be used to produce certain implants as a raw material. This polymer has excellent mechanical properties, biocompatibility and properties close to the human bone. It corresponds practically to the elasticity coefficients and provides a more effective implant function [3-5].

The use of PEEK has increased substantially as a spine material for arthrodesis in recent years. Percentages of each material are obtained over time, with emphasis on data related to PEEK. Due to its stability, biocompatibility, radio transparency and critical mechanical properties, it supports PEEK biomaterial to be suitable for solving problems related to some applications and solutions for implants [6-8]. PEEK can be made available by suppliers in powder or granules, which are later converted into products through extrusion moulding and injection processes. Other forms of presentation of this raw material are bars and tubes made by extrusion or sheets moulded by compression [9-11]. These can also be reworked to obtain the desired final product. At first, PEEK is beige, but when it is associated with carbon fibres to support mechanical resistance, the material from this mixture is visualised in black. PEEK can be combined with some additives to create some composites. Composite can be defined as a material consisting of two or more distinct phases, and each of them maintaining its peculiarity and properties, both physical, biological and mechanical [12-14]. Among the first additives used to increase PEEK strength and stiffness are glass and carbon fibres. The configuration of PEEK with carbon fibres is a vital interface that effectively distributes and transfers the stresses from mechanical loadings between the fibres and the polymer matrix [15-17]. When associated with carbon fibres-polyetheretherketone (CFR-PEEK), characteristics depend on the length, size and orientation of the fibres used. This type of composite has been currently used in implants for spine and joint replacement. In addition to some additives being intended for the biomechanical function of the material, others are used for various biomedical purposes [18-20].

Furthermore, an example of an additive with the properties mentioned above is barium sulfate. A radio pacifier mixed with PEEK gives better visualisation and contrast in *medical imaging*, facilitating radiological control during and after surgery. Studies are being conducted to investigate the combination of PEEK with some bioactive materials, which promote bone growth around the implant and improves its fixation [21-23]. An example is hydroxyapatite (HAp), which can be represented using the chemical formula $Ca_5(PO_4)_3OH$. HAp is presented as the reference material for biomaterials, as it exhibits excellent biocompatibility, osteoconductivity and biological activity, besides its similarity with the mineral part of teeth and bones. It allows for the proliferation of fibroblast and osteoblast cells, which do not distinguish it from the bone surface and hydrophilicity, thus allowing their surface to wet with weight [24-26]. Despite all the advantages exhibited by HAp, its clinical use is limited due to its slow biodegradation. Studies carried out over long periods have shown that HAp begins to be gradually reabsorbed after 4 to 5 years of implantation. Resorption is a desired characteristic for biomaterials in which the degradation process occurs concomitantly with the replacement of the bone information [27-29].

Due to the increasingly competitive market for these implants, the quality of the product must be improved, combining the facilities promoted by the support material, besides promoting a competitive price [30-32]. The polymeric injection process can increase production volumes of intervertebral spacers and improve the production and production of products with higher aggregate quality. It is an excellent alternative to those who have been long-term seeking increased productivity and quality, despite high initial costs for acquiring tools and machinery [33-35]. In addition, the technique of additive production (AM) represents significant progress in printing complex

geometries for a 3D (3D) bone structure and an essential step towards geometrical optimisation of bone 3D printing. Studies predict that this technology will be ready in around 2-3 years for industrial applications. The bone implant of the PEEK structure has shown that it increases bone output in several respects, such as four times the respective capacity and twice the area capacity of a solid electrode block [36-38].

Importantly, this groundbreaking approach is critical to applications in the cell and medical equipment industry. This study is well integrated with biomedical devices that require miniaturised scaffolds. This work for bone implants due to their low weight and high capacity will also benefit a Non-biological Cell Spine implant.. Therefore, the main objective of this current study was to demonstrate the spine implant process in the manufacture of an intervertebral spacer model, thus showing some differences between these manufacturing processes. This study aimed to improve knowledge and provide guidance for such simulations through various grid structures, simulated by finite elements analysis (FEA) software. Include the elements also with the homogenisation approach and has joint strengthening effects on homogenised characteristics. This was achieved by evaluating the unit cell homogenisation method with a 3D component and comparing the methods used to determine whether their deformed predictable structure matches. This more critical and complex investigation was made up of only selected cell units of isotropic beam-cell structure material with a linear elastic deformity.

2. Methodology

Variations in fused deposition modelling (FDM) technology have led to the manufacture of scaffolds in biometrics PEEK. Although it does not use a laser, another recent PEEK prototyping technique is electron beam melting (EBM). The powder is dispensed under an electron beam to be cast according to the part drawings. With these fast PEEK prototyper technologies, large pores and functionally graded pores can be controlled (FGPD). These changes using high energy beams also have allowed the production of ceramic pieces, which could soon lead to the manufacture utilising high dimensional and geometrical spatially controlled pores of the implant volume of pure calcium hydroxyapatite (cHAp) scaffolds. The sample was also subject to high laser power, resulting in vapour releases. These problems have been resolved using the test-and-error method, reducing the dust temperature on the building platform. Double scans with a 1mm hole laser in the field of up until 10 layers (~ 2.5 mm) were built to remove the roulette speed and increase coating thickness.

The structure was also placed in a stove which was heated in a vacuum chamber slowly to 320°C. It was just below 350°C but heated sufficiently to vaporise organic materials of the structure and left PEEK only behind. The heating method was also known as pyrolysis since the process evaporated 80% of structural material and its dimensions but maintained the form and proportions. The final contraction explained, in large part, why structures can be made very small.

The software Mountain 8 Premium used for reproducing, developing and delivering images was used in the 3D anatomical region of interest via unique imaging systems. 3D printing Mode was converted into a STL shape for AM equipment to print a structure that effectively replicates the exciting anatomy of the physical prototype (Fig. 1). In health applications, this material model is known as a bio-model [38-40]. The dust layer is manufactured as in AM technology as in FDM. Still, liquid glue action achieves dust adhesion at high temperatures, such as at room temperature with SLS instead of laser beams. The selection of the release of melted

powder resin was made with the printhead, similar to inkjet printers for paper printing [41-43]. Dimensional accuracy was achieved with AM, and it is often used as prototypes or imaging concepts.

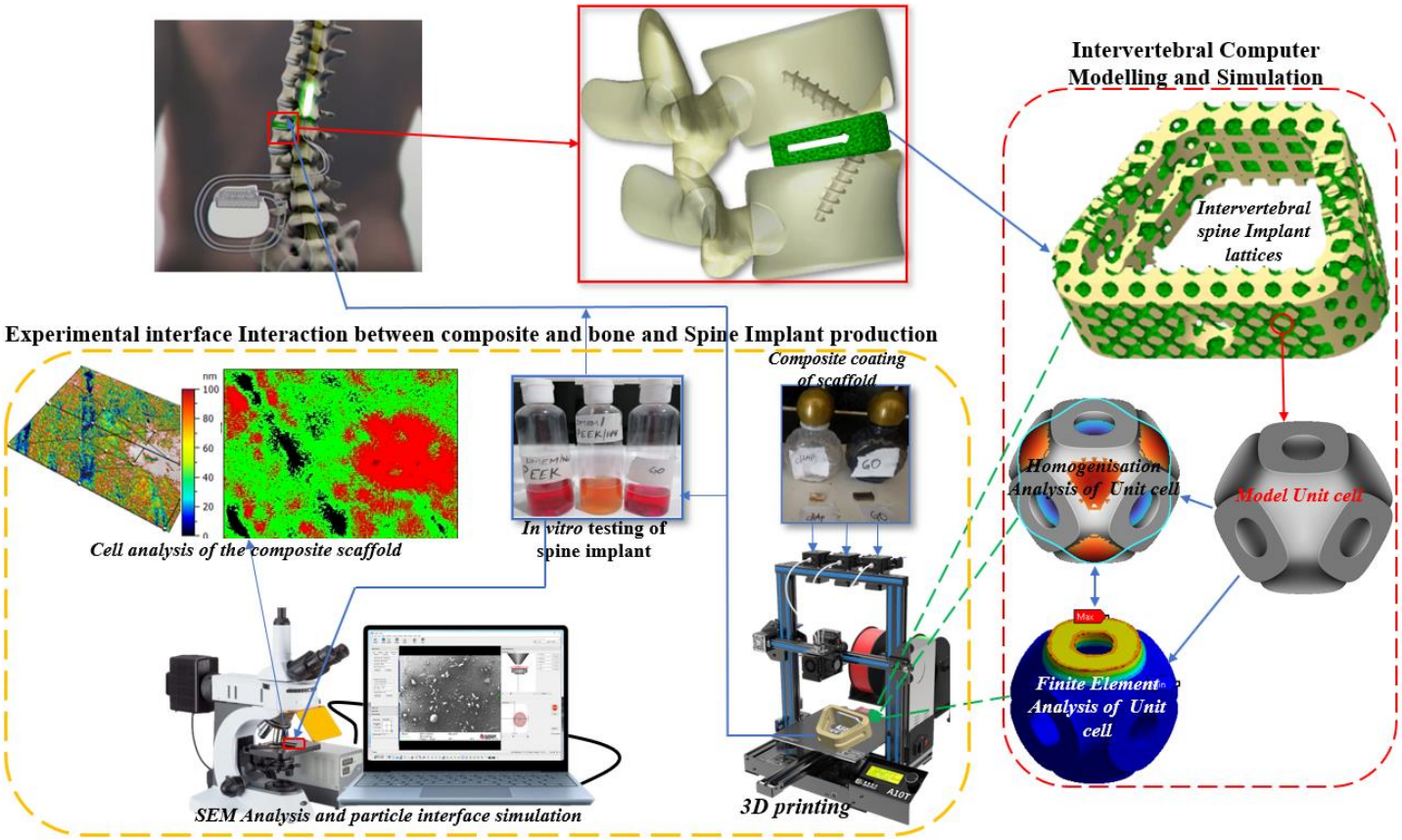

Fig. 1. Sequential experimental set-up for the system workflow for 3D printing in vitro and biological evaluation of the PEeK composite for biomedical tissue engineering scaffolds, the production of cell propagation and bone-implant attachment in FDM.

To use the correct techniques and parameters for PEEK processing, specific guidelines of the supplier must be followed and other used polymeric materials. Some specifications presented by the manufacturer have in their product line PEEK-OPTIMA, a raw material exclusive for use in implants. The raw material was made available by the supplier in granules, in packages free of external contaminants, with double sealing and equipped with a system where possible counterfeits can be identified. The raw material initial conditions must be maintained to have a "pure" and reliable product, without contaminants, during all processing stages. Before using PEEK for subsequent procedures, drying was performed to remove moisture from its granules, reaching around 0.5% of the total weight. It was recommended to use raw material with a maximum of 0.1% moisture before the injection process. This value was obtained using an air circulation oven. The granules were spread in clean trays with a maximum height of 25 mm to get the best drying results. Another important factor observed was the cleaning of the oven, which was free of any contaminant. Due to the high risk of contamination, the leftovers from the polymer processing was not used, and it was properly discarded.

3. Design of lattice nanostructure

A layer-by-layer object was created for 3D printing, also known as AM, which enabled creating structures that could not be made using conventional subtraction methods, including graving or grinding. Composite materials are used to produce ultra-fine 3D designs built by AM for bone implants. Therefore, it made a 3D lattice, with beams nanometers long and wide and too small for the naked eye to be seen. This material showed unusual, often surprising properties and created an exceptionally soft bio compound after compression returned to its original form [44-46]. For the manufacture of higher and lower capacity porous PEEK, 3D printing was used. A new 3D printed bone structure process was built (Fig. 2). In PEEK, the porous architecture structure can lead to increased body fluid injection capacity.

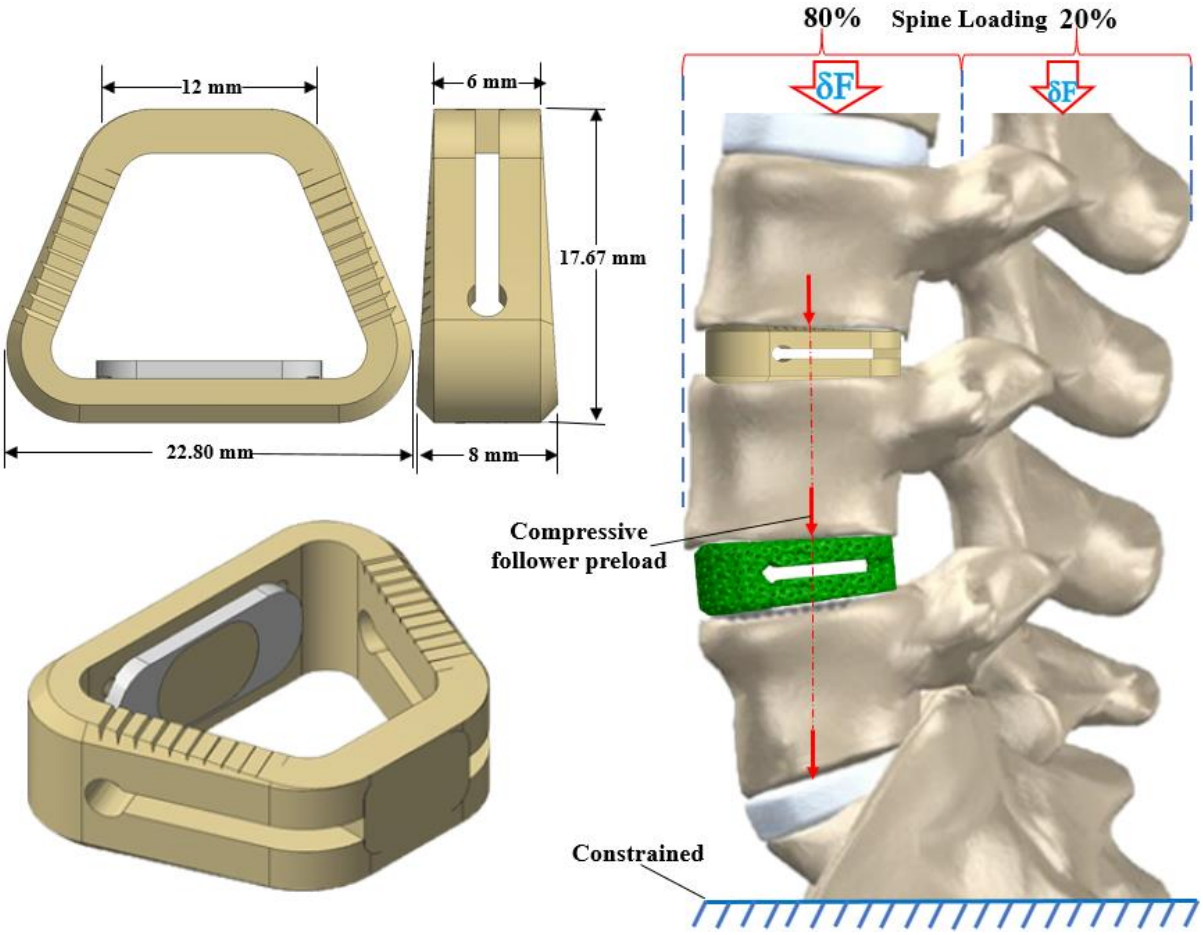

Fig. 2. Design and implant the spine cage and lattice structure in vertebral bone, showing applied load distribution in the human body and fixing support.

4. Mechanical testing

A universal Intron test machine was used to conduct a tensile test at a constant displacement of 1 mm/min and a temperature of 25°C. The load rate was reduced to make a comparative analysis of more versatile and mixable materials more straightforward. Ansys and Creo software packages were also used to calculate the strain, tensile power, percentage elongation and modulus of the 3 mm thick and 32 mm long composite specimens. Tensile test was conducted according to ASTM D638 standard, and it included rGO specimens of 1-5 wt%. AM is a project focusing on the research, development and dissemination of virtual and physical prototyping technologies, which

use surgeon AM technology. A Mountains MAP Premium 8.2 Surface Digitiser software for virtual prototyping was used and distributed free. Surgeons are familiar with 3D technologies to plan surgeries, using virtual bio-models constructed from tomographic images.

Similarly, supplies with physical bio-models were made with AM from the virtual bio-models to ensure that surgical planning was done most realistically or possibly. In physical bio-models, marking of the cuts was not only performed. Another application of these technologies is the anatomical moulding of implants. The effects of AM on structural parameters are presented to examine the impact, and two parametric studies were carried out. The first is for common form, and the second for the angle of construction and the raster corner of the extrusion material. We built surrogate models based on parametrical studies in homogenisation procedure used intercalated structural values. Homogenisation procedure for evaluating two mechanical characteristics, elastic characteristics of steadiness matrix and yield. We use a multi-scale method to derive homogenised mechanical efficiencies. The whole structure of the lattice is macro, and its representative cell is defined on a micro-scale. Combining strain energy and resulting strength after deformation at both scales, the effective mechanical qualities are also derived. We include the proposed homogenisation process suggested for the AM process and the joint stiffening effects of semi-rigid, efficient collaborative frame elements. The parameters of the structure efficiency are determined by substitute models in specific grid structures based on strut diameters and corners. This allows the analysis of as-made voxel models, which can normally last up to several hours for each stroke, depending on the resolution of the voxel models.

5. Results and discusion

With a rough structure, the sintered material has high porosity and low mechanical resistance. To confirm biocompatibility of nylon-6 and build scaffold pores of 800 μm using AM, scaffolds were tested in the AM equipment and nylon was observed to be biocompatible. The platforms were supplied with pores with a cubic geometry of 500 μm. In case of the mandibular bio-model, pores were also obtained at the side of 700 μm cubic geometry and 500 μm at the wall. The construction of nylon-copper composite parts was also part of other tests conducted at InVesalius 3. Although copper was not bio-compatible, experiments have shown that polymer-metal composites can be quickly prototyped or ceramic prototyped. The profile derived parameters, which shown the roughness profile of the PEEK-rGO-cHAp scaffold, are shown in Fig. 3, according to the ISO 4287 standard.

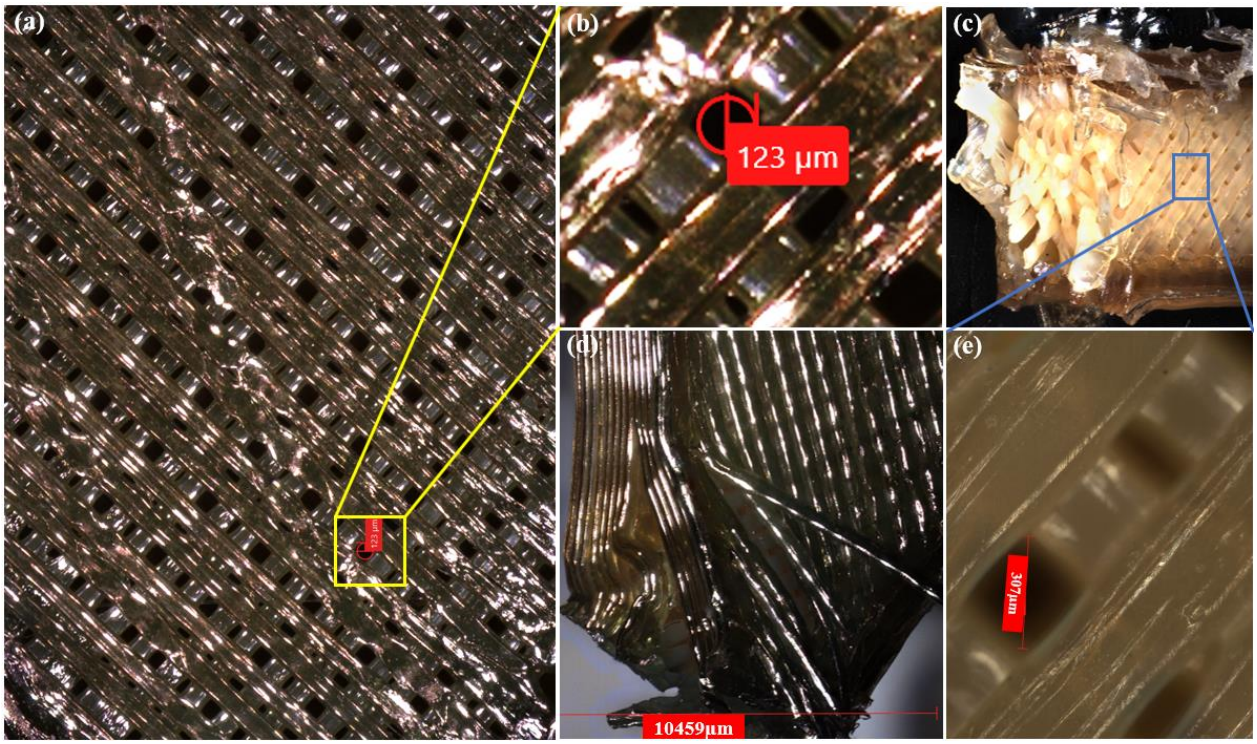

Fig. 3. Microscopic reference sample demonstrated a significant void development in the centre porous PEEK-rGo-cHAp composite, due to the weight reduction of the sample: porous material magnification element at (a) 100x, (b) 50x (c) 100x, (d) 500x porous material magnification at 712 mm (al) 534 mm and (e) 1000x pixel magnification at a resolution of 0.2225 mm/pixel microns with exposure time of 1.2872 ms.

5.1. *Lattice structures*

Lattice designs were created in PTC Creo Parametrics 7.0 and modified in ntopology, and Fine homogenisation simulated with the Ansys workbench and ntopology software (Fig. 4). After heating the 10 mm stainless steel starting plate to 330 °C, selective electron beam melting was used for directly building bars with 10mm supporting structure on the preheated starting plate. The entire procedure was conducted under a vacuum controlled by high pure helium, which was used as a regulating gas to prevent powder charging. The powder recovery system removed semi sintered powder particles thoroughly from the built-in grids [47-50]. The lattices were polished in parallel on compression surfaces with a maximum difference of 10 µm. The mean area for the system was 17.7, 32.9 and 21.1 mm^2.

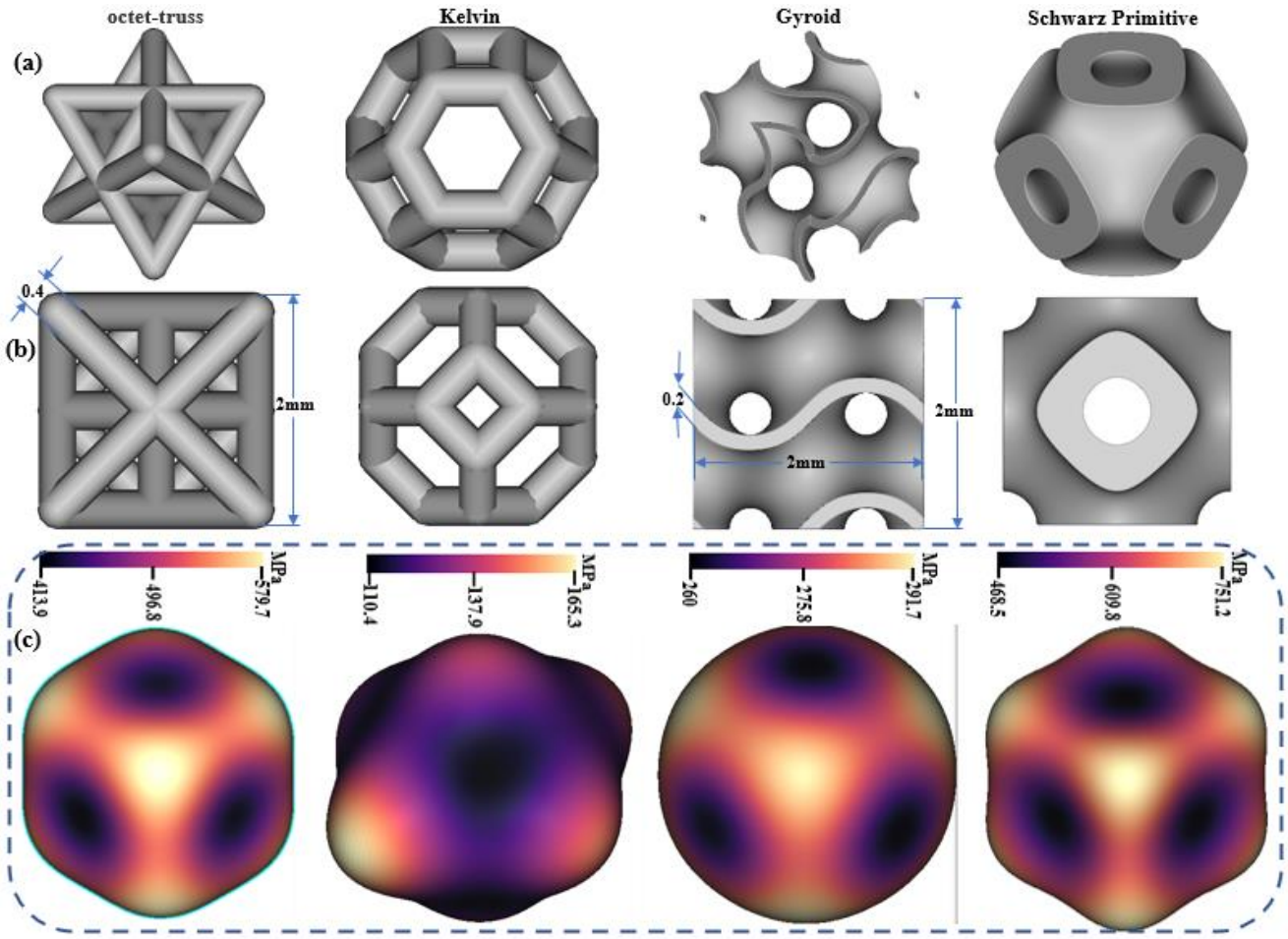

Fig. 4. CAD design lattices for spine intervertebral implant application, showing (a) 3-dimensional view (b) 2D view, and (c) lattices homogenisation.

Besides, this current integrated well with cell devices for biomedical applications that involve miniaturised scaffolds [50-53]. The microdevices, a non-biological cell, also supported this work. Due to the low battery weight and the high capacity of the process, the bone implant can be used on a larger scale. The four lattice structures with a cell size of 0.4 mm of octet-truss and kelvin lattice and two 0.20 and 0.25 mm of Schwarz Primitive structure and primitive were designed and analysed (Fig. 5).

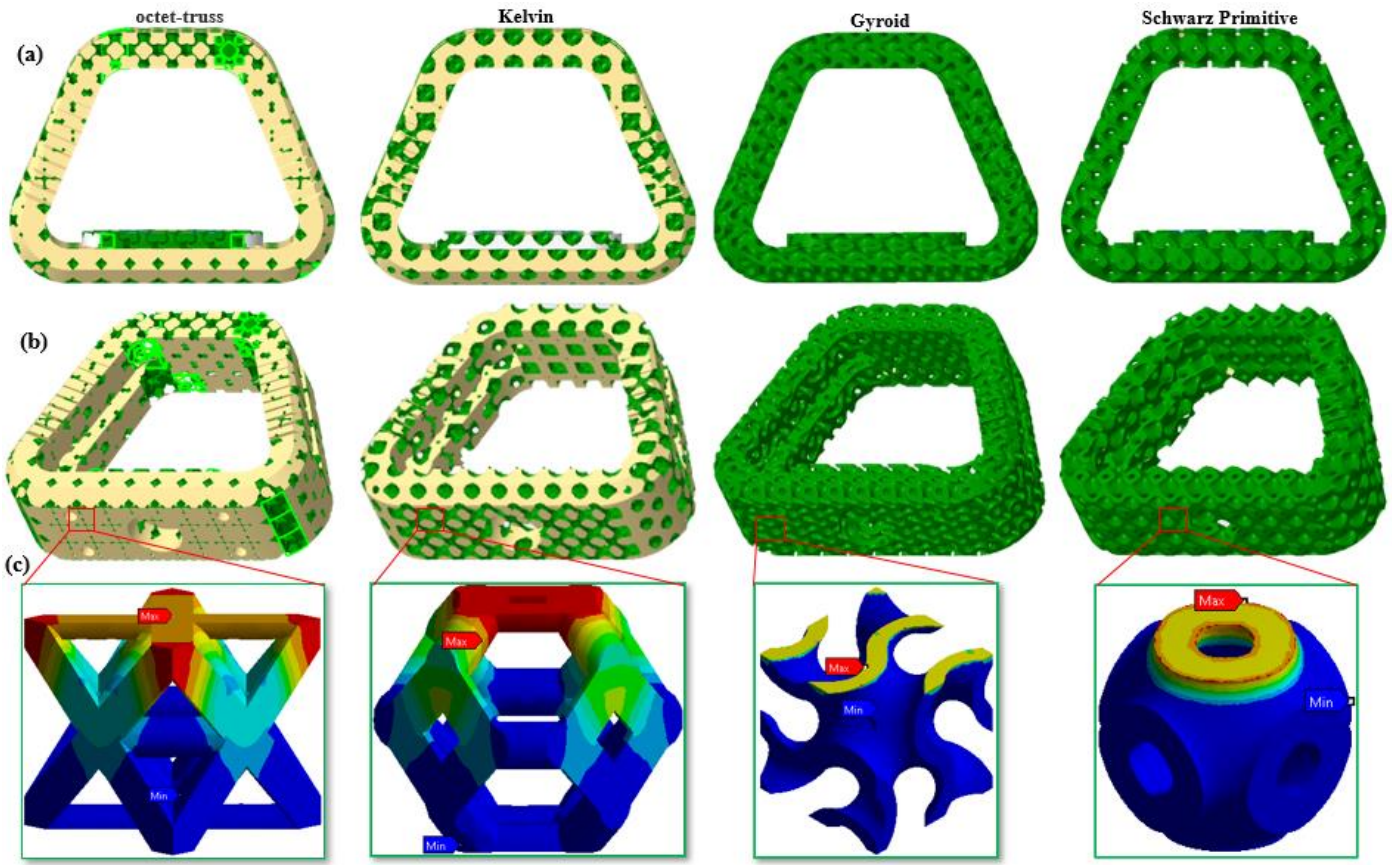

Fig. 5. The four lattice structure application to intervertebral spine bone implant of PEEK composite, depicting (a) side view, (b) 3D view of the spinal implant and (c) displacement simulation of each unit cell in application to spine implants.

5.2. ***Homogenisation Elastic Properties***

Figure 5 shows the steps to homogenise the elastic properties of this product. Comparing the deformation energy of the micro and macro scales the elastic properties of the network structure were determined. To define the representative unit cells at the macro level, we start by defining the critical junctions and time vectors and then classify the dependent and independent nodes at the comma level, as shown in Figures 6 and 7. The dependent node position vector is represented by the linear combination of the free node position vector and the entire product of the period vector. All internal nodes are therefore independent and always slave nodes at the cell limits of the unit. The four-channel views and the figure shows each of the key positions in the unit cell. The macro-deformation displacement field causes internal stress in each micro-level rod. When the internal stress in the tire axle reaches the elastic limit of the material, the bundle structure will fail. Therefore, we define the homogenisation flow resistance as the minimum macro stress that initiates flow at any strut in the unit cell. Figure 5 shows the general homogenisation procedure for the flow limit. The process starts with the determination of the given macroscopic stress field of the node displacement vector. The actual vector is subsequently removed from the vector of the Microscopic Node. A balance of elements is used to determine the basic force vector. Considering the normal and shear distribution of the cross-section, initial stress is evaluated at three points and a maximum of two distances between the centre and the midpoint of the cross-section. At the point of maximum slackness, we

set the shear force to zero. However, the maximum stress of Mises is chosen for the next step by using the fundamental shearing force in the centre.

5.3. *Modulus of elasticity*

Figure 6 shows the results of a parametric study for the standard homogeneous elastic limit. Like elastic properties, elongated Unit cells are less sensitive than folded unit cells to joint properties. Two components can express the inner stress in the connection rod. The first concerns the normal strength, and the other relates to bending cells in an extended unit, most internal stresses develop in the first stage (F / A), a term that has nothing to do with the length of the connecting rod. Therefore, the effect of seal properties on tall unit cells is limited. The results of the cubic cell in Figure 6 support this, showing that the elastic limit depends only on the diameter of the connecting rod. Standard features in this unit cell do not affect resistance. The cell of octal beam cells in Figure 6 are also similar to results for high-force joints in a cubic cell. Since the unit cell is made up of a tilted column that can act as a straight line, low rigid joints affect the perspective.

On the other hand, the results of the unit cells in Figure 6 for Schwarz Primitive were dependent on the joint properties. The trend is more difficult than the two other dominant expandable cells. For stability: the greater the outcentricity, the higher the elastic boundary. The reason is that a shorter framework length leads to less bending time and makes the body structure more external.

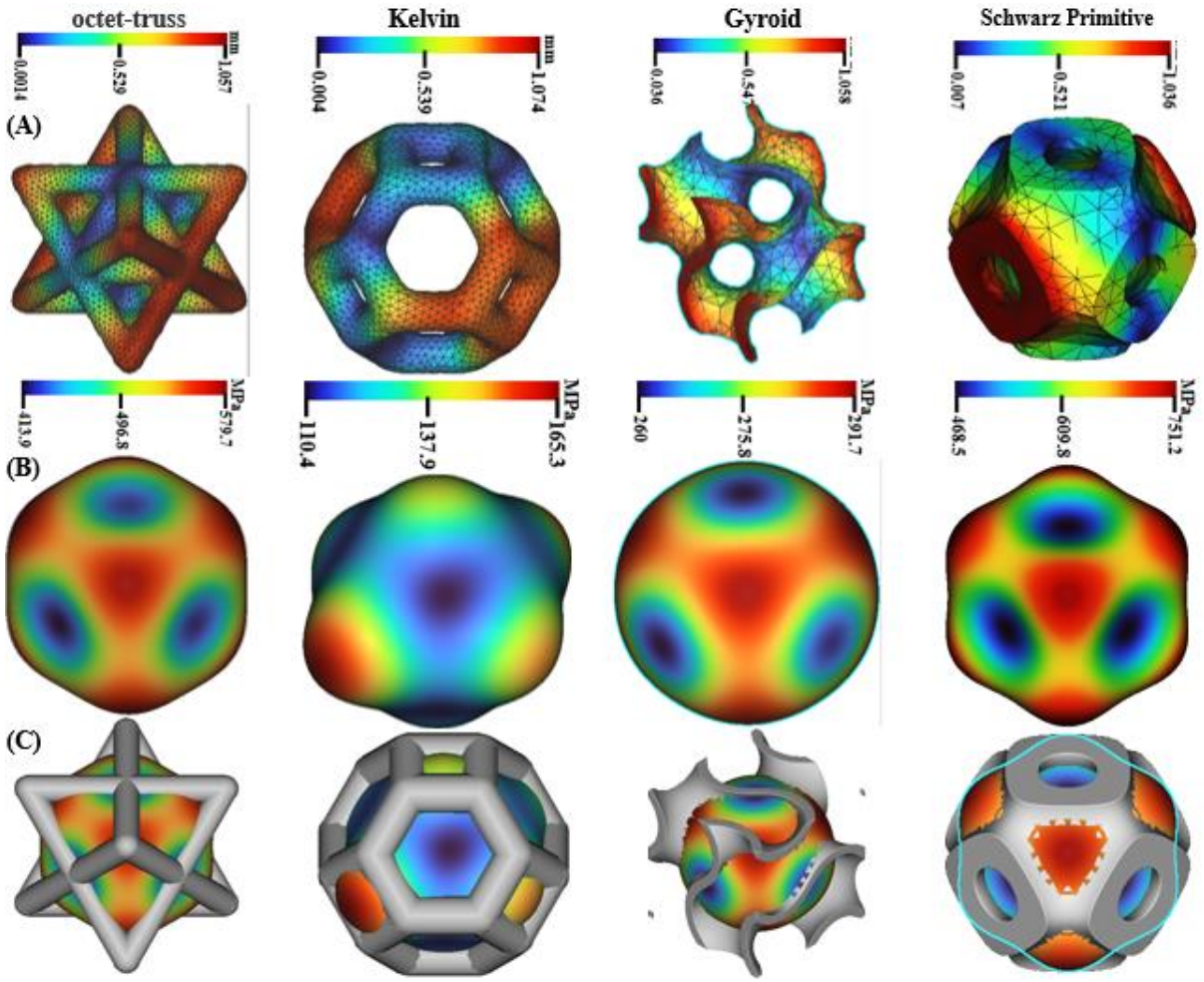

Fig. 6. (a) Directional cell displacement stress, (b) directional homogenisation of Young's MPa and (c) unit cell unit unit homogenisation behaviour.

5.4. Homogenisation Validation

To first study the effect of the angles set during the AM process, we design four-cell cubic samples. Examples of cubic cell properties can be found in Table 4 Every cubic cell instance is of the same size in this sample set. But the address of the unit cell is turned. We have created three Schwarz Primitive unit cell samples. Table 5 shows an example of a Schwarz Primitive unit cell. For instance, all Schwarz Primitive cells have the same cell structure. But with different sizes, we produce samples on an Intamsys Funmat HT PEEK Ultem 3D printer using PEEK material, layer thickness 0.254mm, and then perform a tensile test using an Instron tester. We used three homogenisation methods for comparison purposes: Proposed discrete homogenisation with members of the traditional Euler structure and asymptomatic homogenisation [54-57]. A parametric study determined the effective structural parameters for the proposed approach. Two mechanical properties, elasticity module and flow resistance are evaluated and compared with the test results. The approximate elasticity and flux resistance in the first sample are shown in Figures 6 and 7. The results are normalised from the test results—the maximum and the minimum modulus of elasticity. The results obtained from the test were 5790.7 MPa (413.9 MPa), 165.3 MPa (110.4 MPa), 291.7 MPa (260 MPa) and 751.2 MPa (468.5 MPa) octet-truss, kelvin, gyroid and scharz primitive, respectively. (Fig. 7)

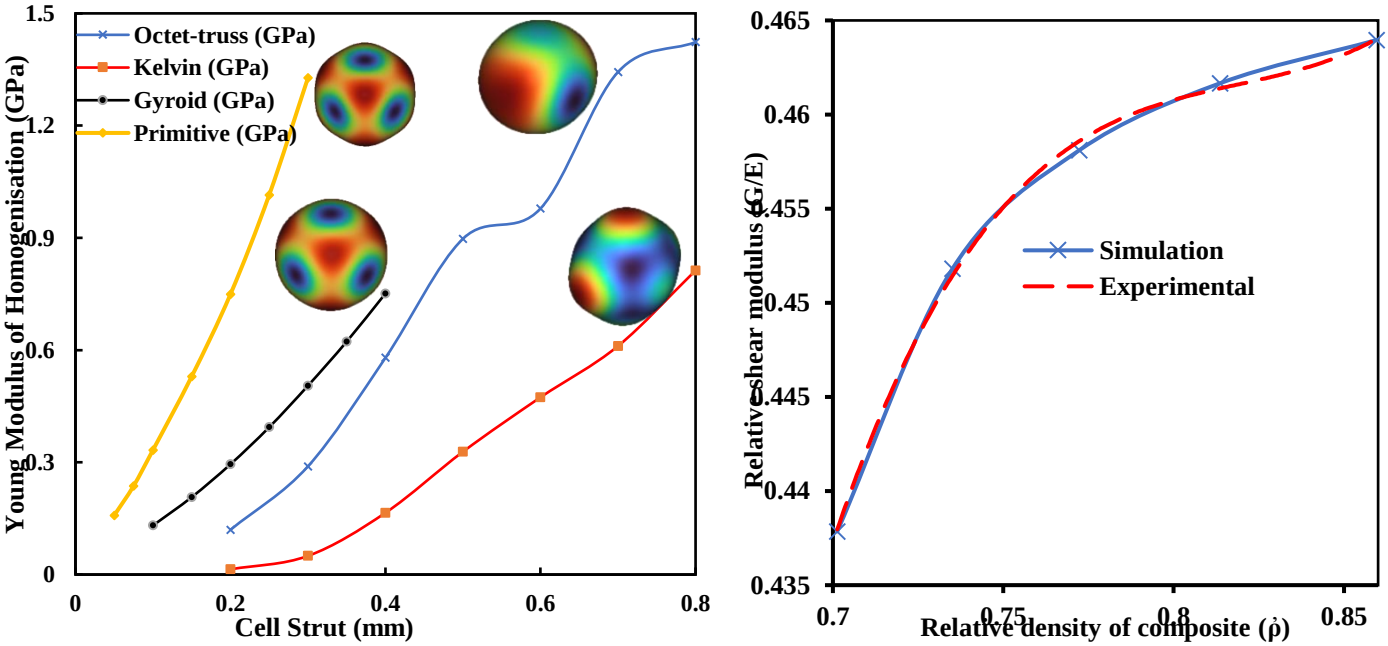

Fig.7 . (a)Young modulus of homogenisation of the four lattice structures on the cell strut thickness (b) the Relative shear modulus to relative density of composite

The proposed approach to compare the modulus of elasticity at most rotation angles leads to a precise process. They are configuring the Euler structure results in more restricted predictions. The results of the silent homogenisation method show a big error in some cases. This method overestimates the rigidity of the network structure. As the asymptomatic homogenisation method uses solid elements that define geometric details, including joints, intact geometry is more rigid than distorted. Therefore, the estimates are slightly more stringent

than other estimates for the elastic limit. The use of a semi-rigid link structure member can significantly reduce the estimation error. The traditional method of homogenisation with structure members tends to overestimate the strength of the grid structure about two times as the technique has a more significant total diameter than the effective focal rod diameter. The maximums estimated stress result was less than the estimate of the approach proposed, the semi-rigid junction frame. The evaluation of the strength of the truss structure was therefore extremely important. However, the asymptomatic homogenisation method considered the elastic limit significantly below 79%. Due to asymptomatic homogenisation, solid elements that develop unrealistic stress concentrations in the acute geometry to which the columns are connected were used, and linear analyses were performed. This resulted in a decrease in the predicted elasticity limit. Figure 8 shows the modulus of elasticity and the average estimates for the elasticity limit in different thicknesses (t_i) of the cell octet-truss, kelvin, gyroid and scharz primitive of lattices structure samples. Each of these thicknesses gives different mean and range young's modulus of the test for 0.4 struts for the beam lattices and 0.2 for the formula lattice were 496.8 MPa (165.8 MPa), 137.9 MPa (54.9 MPa), 275.8 MPa (31.7MPa) and 609.8 MPa (282.7 MPa) octet-truss, kelvin, gyroid and scharz primitive respectively. The results show that the proposed approach of homogenisation overestimates the elasticity module due to the column diameter. Furthermore, the use of structural elements from Euler for unitary primitive Schwarz cells resulted in overestimating rigidity. The member of the Euler framework overestimates its rigidity by ignoring shear deformation, as the primitive Schwarz cell is curved and the neck has a low taper proportion. The asymptomatic homogenisation method provides a greater elasticity module for the same reasons mentioned in the previous section. For flexible limit estimation, estimates for other discrete homogenisation methods will be different. Since the approach uses entire geometry, the effect of the Additive manufacturing process cannot be combined with the resource forecasting process.

5.5. Homogenised Stiffeness Mechanical Properties

This section describes the effect of joint hardening on their mechanical properties. We study parametric in three topologies of the cubic octet and Schwarz Primitive cell. Tension dominates the first two cells, and bending is dominated by the other. Figure 7 shows the topology of the selected unit cell. Due to the periodic arrangement, duplicate edges are not included in a modified unit cell. The range of the three parameters of the structural elements is shown in Table 3, unit cell established at 5mm. This substance is PEEK with a modulus of elasticity and elastic limit of 1627 MPa and 22 MPa. Where t_i *is the* thickness of the strut

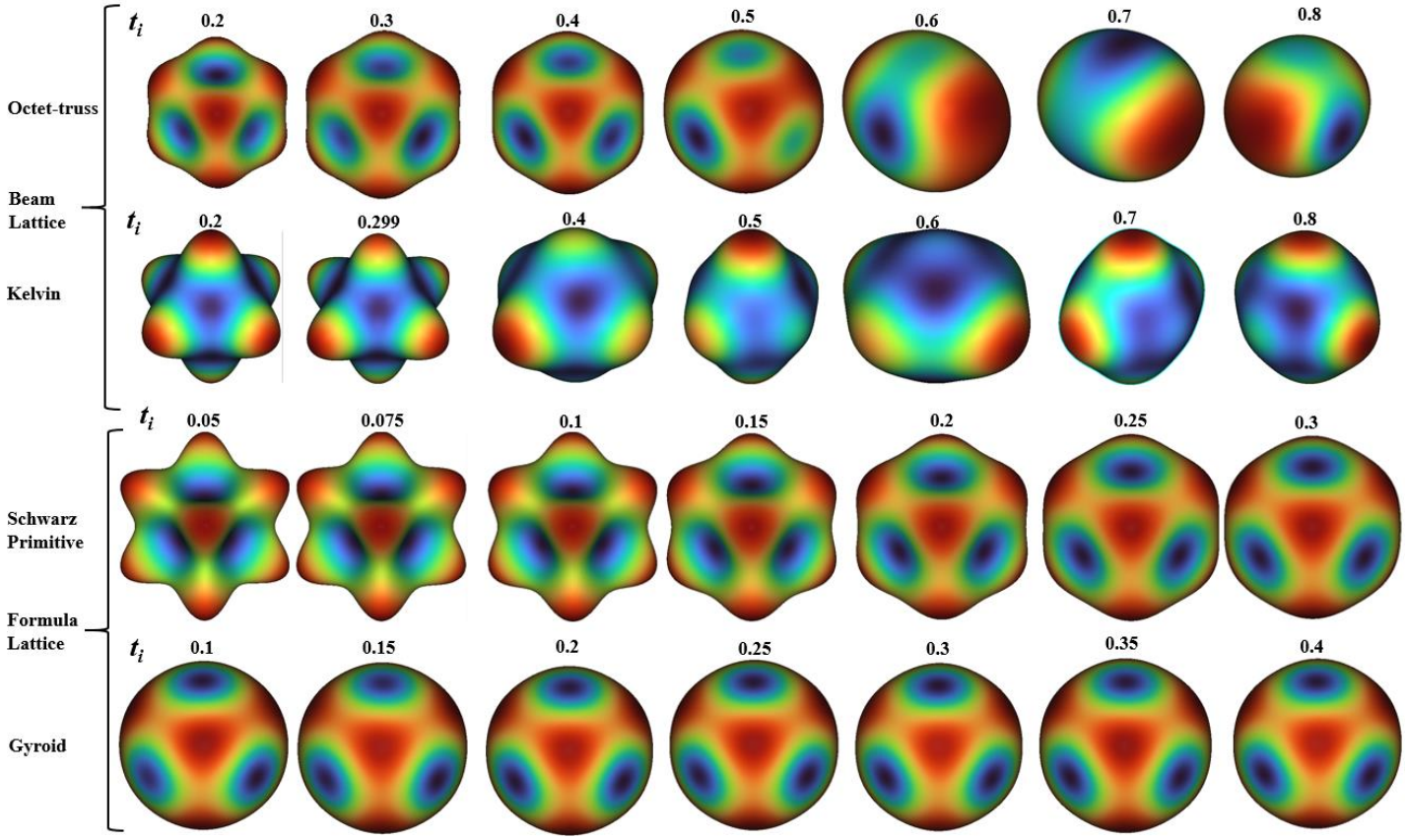

Figure 8 Homogenised Stiffeness Mechanical Properties of different thicknesses for the lattice structure

5.6. **Elastic properties**

The standard elastic modules from the proposed approach are presented in fig 8. Based on the results, we can determine two points. First of all, the gate structures in both unit cells become more rigid as fixities and excentricities increase—the bigger and tighter the joint, the faster the door's structure. As a result, the larger and stronger joint reduces total displacement and strength of response. The reduced length also increases the stiffness of the frame area. The structure of the grid is therefore enhanced through increasing fixity and exenteration. Next, a bend-dominated lattice is more likely than a structure of extended grids to change joint parameters. The unit cells of the cube and the octet are dominated, but the Schwarz Primitive cell bends. By contradiction, the results are shown by stretching overlooked unit cells in Fig. 8 are smaller than in the unit cell Schwarz Primitives (0.25 ~ 1.0) when compared with the bending overwhelmed unit cells in Fig. 8. Based on axial and bending rigidity, this result can be explained in the semi-rigid frame element formulation rigidity

The linear region, which corresponded to the area where the specimen underwent elastic deformation, reached a greater tension in the formula cell before the structure collapse began to occur. After a linear deformation, maximum failure was reached, after which either the stress that supported the test micro lattice structures was reduced, or in the formular cell, a plateau was produced where the design continued to deform practically at constant effort value. As for the beam-cell specimens, composed of small beams, the collapse was not homogeneous, but failures were located mainly in the nodes. Densification, after the entire structure of the specimen, collapsed. There was accumulation of the material, which drastically increased the stress of the specimen and produced a high slope curve until the end of the test at maximum capacity of the machine. (fig. 9)

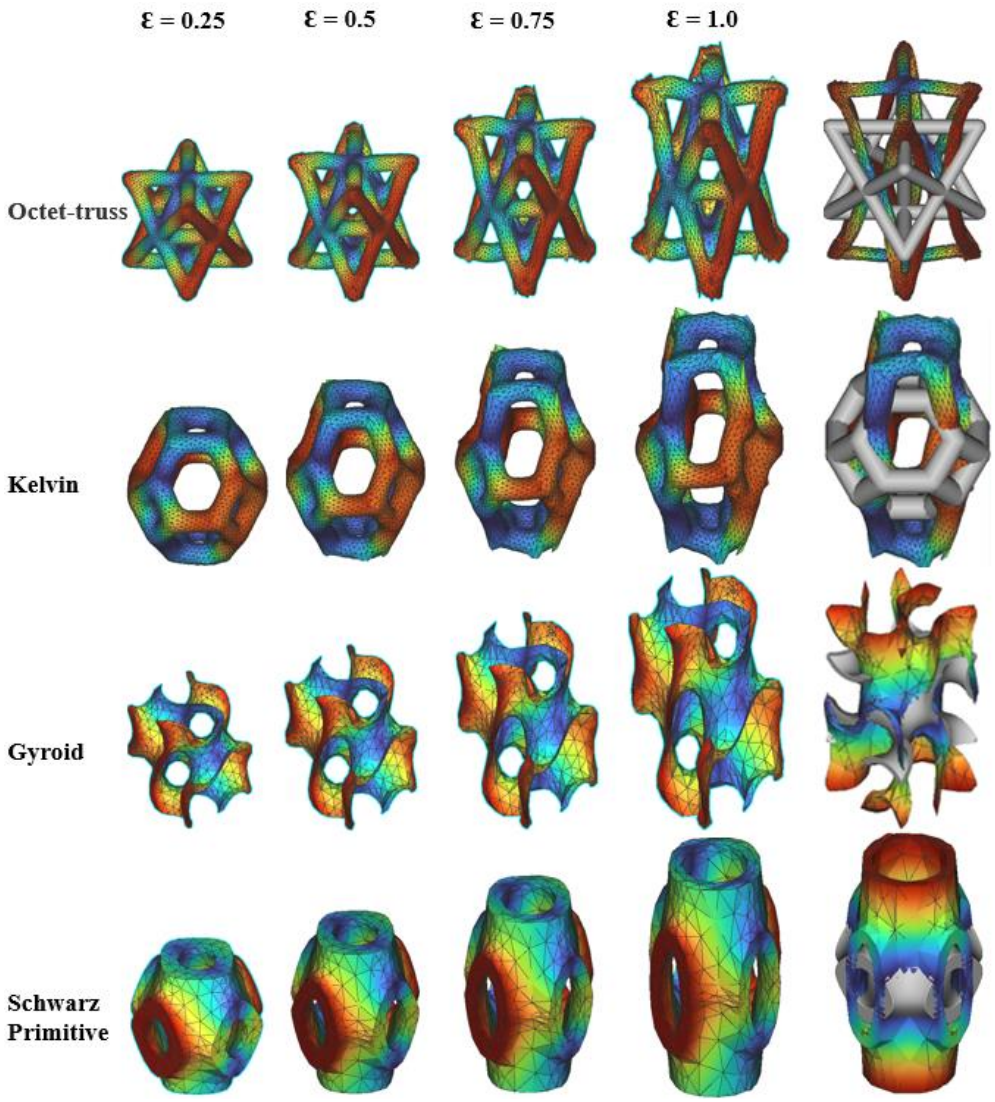

Fig. 9. Comparison of the finite element analysis of the CAD lattice model, showing the stress shift behaviour (mm) of the models in the z direction following load application.

5.7. X-ray diffraction

The PEEK-cHAp sample from opposite 0.1 comprised a grain particle with ramping up to 7.3 mg. The crystallinity amount of the Surface coating procedure exposed skin with cHAp was different from that of the unexposed side from approximately 2%. This behaviour, though subtle, showed that the crystallinity of the surface coating procedure had changed. There was a small increase of crystallinity levels by 2% in absolute terms and 10% in relative terms in layer samples exposed to the surface coating process. Furthermore, for a cHAp-lacquered model, the crystallinity result was subject to only a warm air shock during the surface coating procedure. Considering the analysis methods, there was no interaction observed with potential cHAp particles in the samples taken.

5.8. Microstructural analysis

The results obtained showed that the first group of PEEK samples with a thickness of 2 mm recorded higher values of modulus of elasticity and resistance to bending compared to the group of 1.5 mm thickness samples. In

addition, even if removed, binders can leave pollutant residues and jeopardise HAp biocompatibility by forming inflammatory in vivo agents. A common solution to mix rGO-HAp and PEEK to make scaffolds is composed of composites formed by HAp and biocompatible polymers. The composites were synthesised by heat action. Therefore, AM technology, which was different from other additive manufactures and operated near the polymer melting point, was suitable for directly synthesising the composites. The control parameters of the porosity composed of the HAP grain associated with the HAp-polymer ratio. In general, micrographs and substantial porosity show bio-models that constitute these composites (Fig. 10). When biocompatibility tests have been carried out, the results have been encouraging.

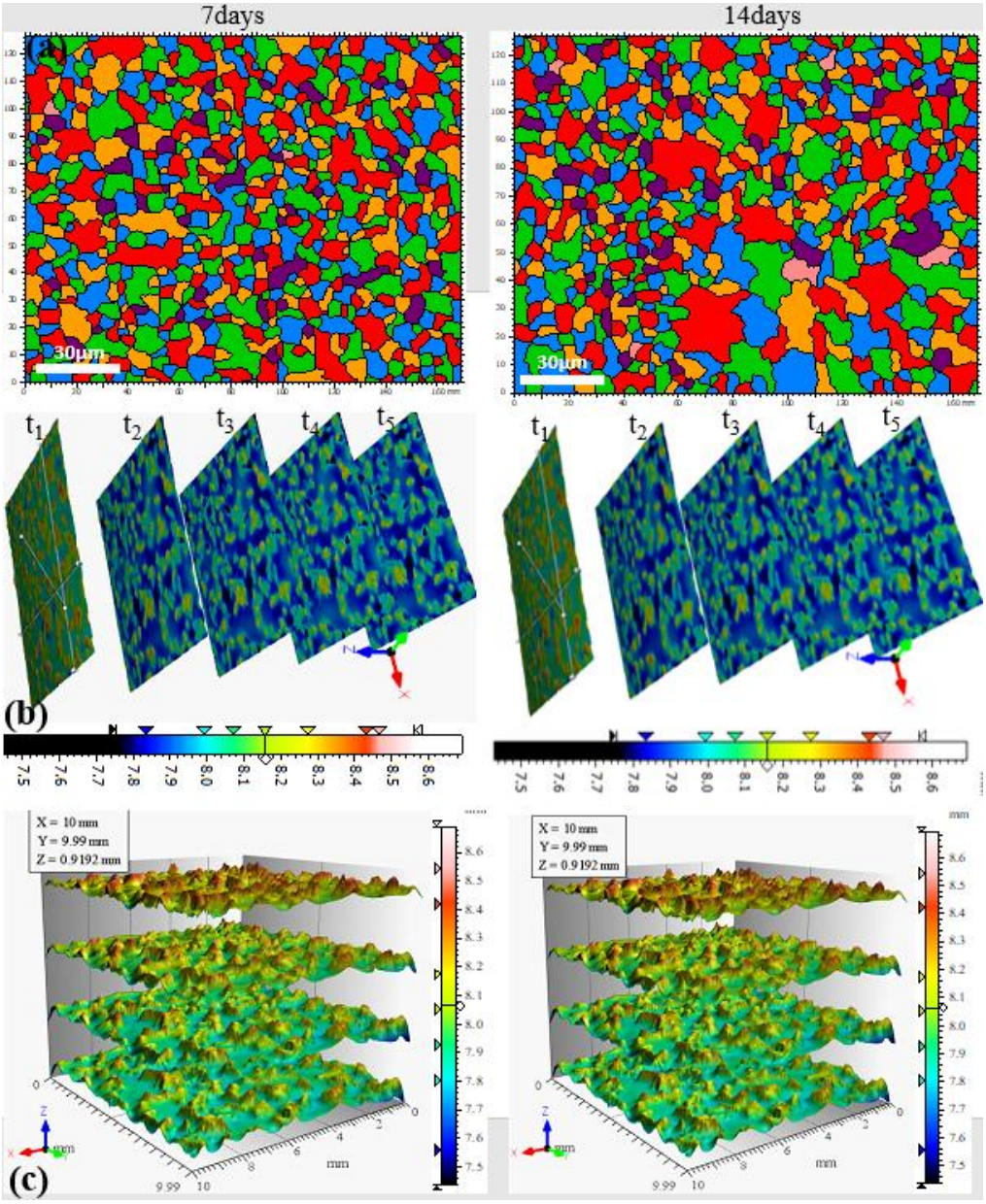

Fig. 10. Cell growth scaffolding development with nanoparticles of PEEK-cHAP coating and 3D-printed bone-implanting scaffolds Biointera representing (a) particle analysis of KL transformation, (b) 4D view of surface time change in series and (c) 4D view of the particle analysis.

Moving forward, Fig. 11 shows the curves obtained from the compression tests. It shows that the curves of the formula cell (Gyroid and Primitive) structures were concentrated in the upper area, while those of the beam cell (Octet-truss and Kelvin) were lower. Three critical points in the evolution of the graph were identified, where there was a direct relationship with the deformation of the piece.

In the definitions of porosity and, in consequence, the definition final mechanical properties of the scaffolding, this control is defined when the load is applied bonding sintering powder. Powder supply technologies are well developed and must be improved on the new AM technology demands. With laboratory screenings, it was possible to choose the powder granulometry range. Consequently, according to a virtual prototype, pores were delineated, which developed after fulfilling the material requirements. This involved smaller laser spot diameters and smaller particle size powder. However, these requirements did not constitute a barrier that could not be transposed, given the high development of lasers and powders. Nanopowder can add great features to implants, such as the controlled release of medications, with the advent of nanotechnology. It then seems that technological resources for AM applications in the biometric sector are available, as the requirement for equipment seems not to be strong. In addition to microfabrication, the AM applied in the biomedical industry will soon provide stimuli leading to what can be known as high accuracy. Addictive production or just quick prototyping of microphones will enable mimicking the trabecular structure of bone in the case of scaffolds (Fig. 11).

5.9. In vitro test

Brian Taylor Office2, Tweed House, Park Lane Swanley, Kent, BR8 8DT, United Kingdom provided a 125 ml microwavable nutrient agar solution (NAS) for cultivation media for agar plates. 125 ml nutrient agar solution is the fastest form of a culture medium from 3-chemical nutrient agar solution. For most experiments, it contained the required compositions. For cell culture medium, it did not require any additional ingredients or biological fluid. It was prepared for about 60 seconds in the microwave bottle can also be done in a hot water bath. The detailed *in vitro* test results for the Nutrient Agar solution of the scaffold are shown in Fig. 11 with a well-elucidated caption.

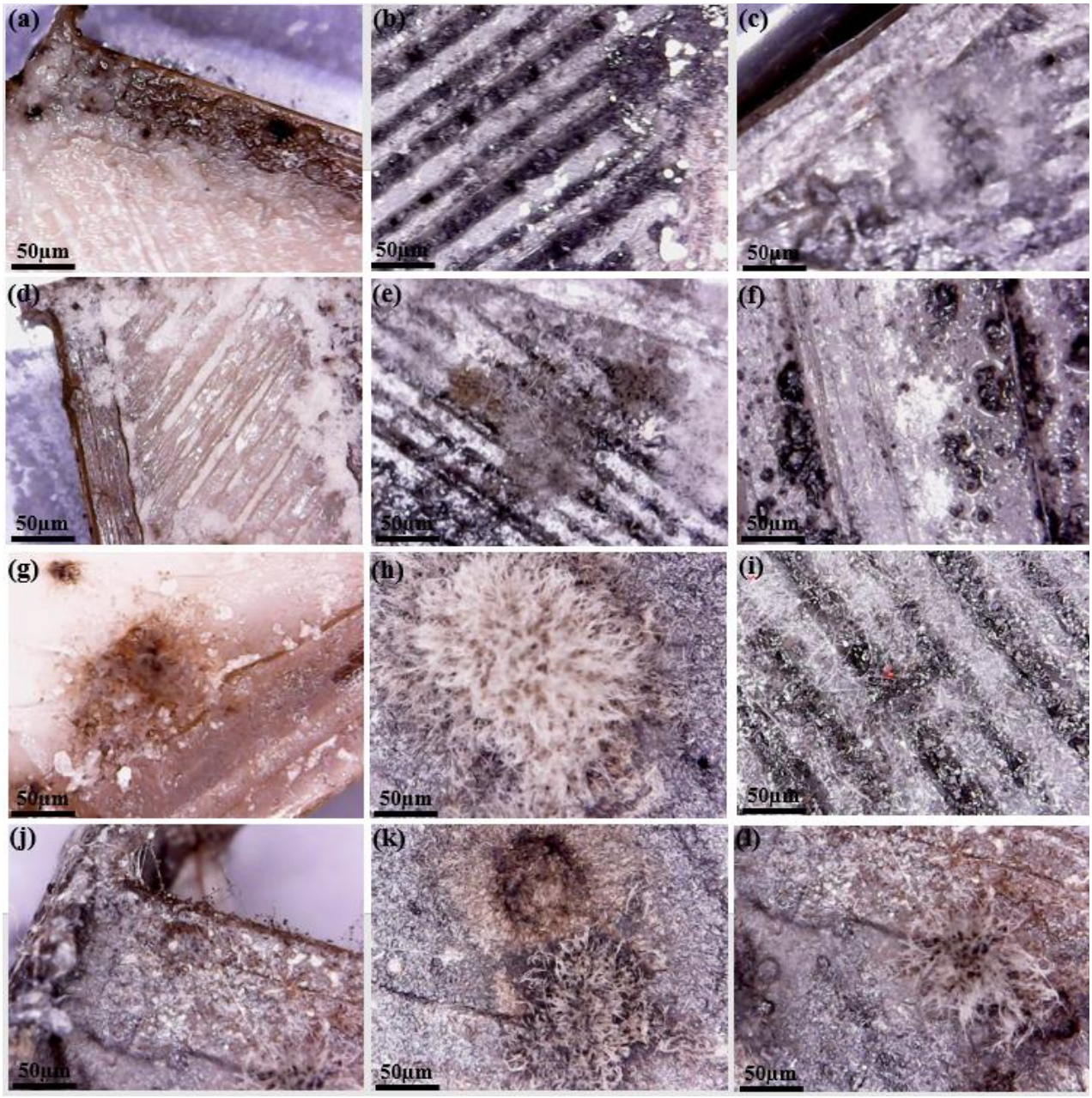

Fig. 11. Live/dead staining of compound sample areas of PEEK FDM 3D-printed cells with Nutrient Agar Cultivation Solution, showing: (a) 24-hour PEEC, (b) 24-hour PEEK-RGO, (c) live cell culture PEEK-rGO and (d) additional cell activity in PEEK during the third to the seventh day. (e) 3rd-7th day PEEK-rGO-cHAp, (f) cell growth on PEEK-rGO, (g) cell spreading to a small dead cell on the 14th, (h) cell spreading to a small dead Cell on the 14th, (f) PEEK-rGO-cHAP cell growth on the 14th day, I cell PEEK-rGO with more spread on the 14th day and (j-l) more dead on the 21st day.

The principles and characteristics in ISO 487 stated the standards of influencing parameters setting used in Tissue engineering for 3D printing with converted scaffolding luminance. The average height of the elements in the raw profile (Rc) with ISO 4287 amendment 2 was 2.94 GL, with a total rawness (Rt) profile height of 13.8 GL, and the mean arithmetical deviation of the ruggedness profile (Ra) was 1.04 GL. Duration of the analysis, the divergence in the root-mean-square (RMS) of the 1,22GL roughness profile was set to 0,0718 with the RRP (Rsk)

skewness and the RP (Rku) skew to 1,82 for the accurate result. Further in vitro test results obtained with the modified eagle medium of Dulbecco were also detailed in Fig. 12 with a well-explained caption.

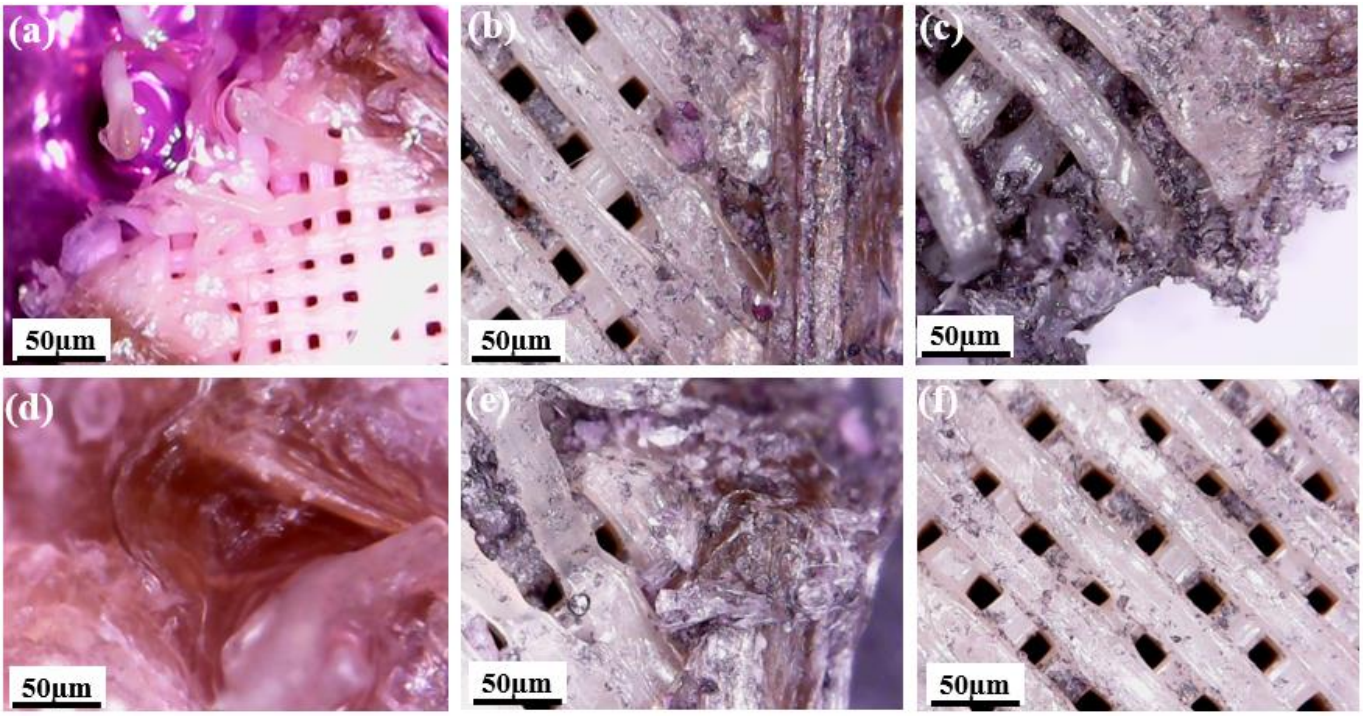

Fig. 12. Sample scaffolded cells after DMEM culture, showing: (a) 50 microns of PEEK after 24 hours, (d) 50 µm of PEEK-rGO-cHAp composite scaffold after 24 hours; (c-d) corresponding magnification of 50 µm of PEEK deposits after three days, (e-f) increased spread of alkalis of cell phosphatases after the 7th day of the PEEK-rGO-cHAp cultivation, Cells attacheted to sample scaffolded surfaces after use of PEEK culture.

5.10. Mechanical and microstructural analyses

A maximum valley profile roughness (Rv) of 120 GL, maximum peak roughness (Rp) of 1.22 GL, complete ruggedness profile (Rh) of 2.41 GL were analysed. The analysis was carried out. Fig. 12 shows cell attachment and proliferation generation of tissue engineering on PEEK-rGO-cHAp grooves during various test days (a) The sample profile is inscribed in the analytical scale by the Gaussian 0.8 mm filter, (b) the sample amplitude roughness profile has been extracted over various days and (c) the number of motifs for particle analysis[57-59]. The frequency spectrum and tolerance limit test for particulate luminance show results of grain analysis in grain/mm^2 of PEEK-HAp of reduced valley depth (Sck) are represented in Fig. 13a and b. The parameters used were wavelength of 0.535 µm with an angular value of -44.49°, frequency magnitude of -44.26 dBc and a phase of 135.6°.

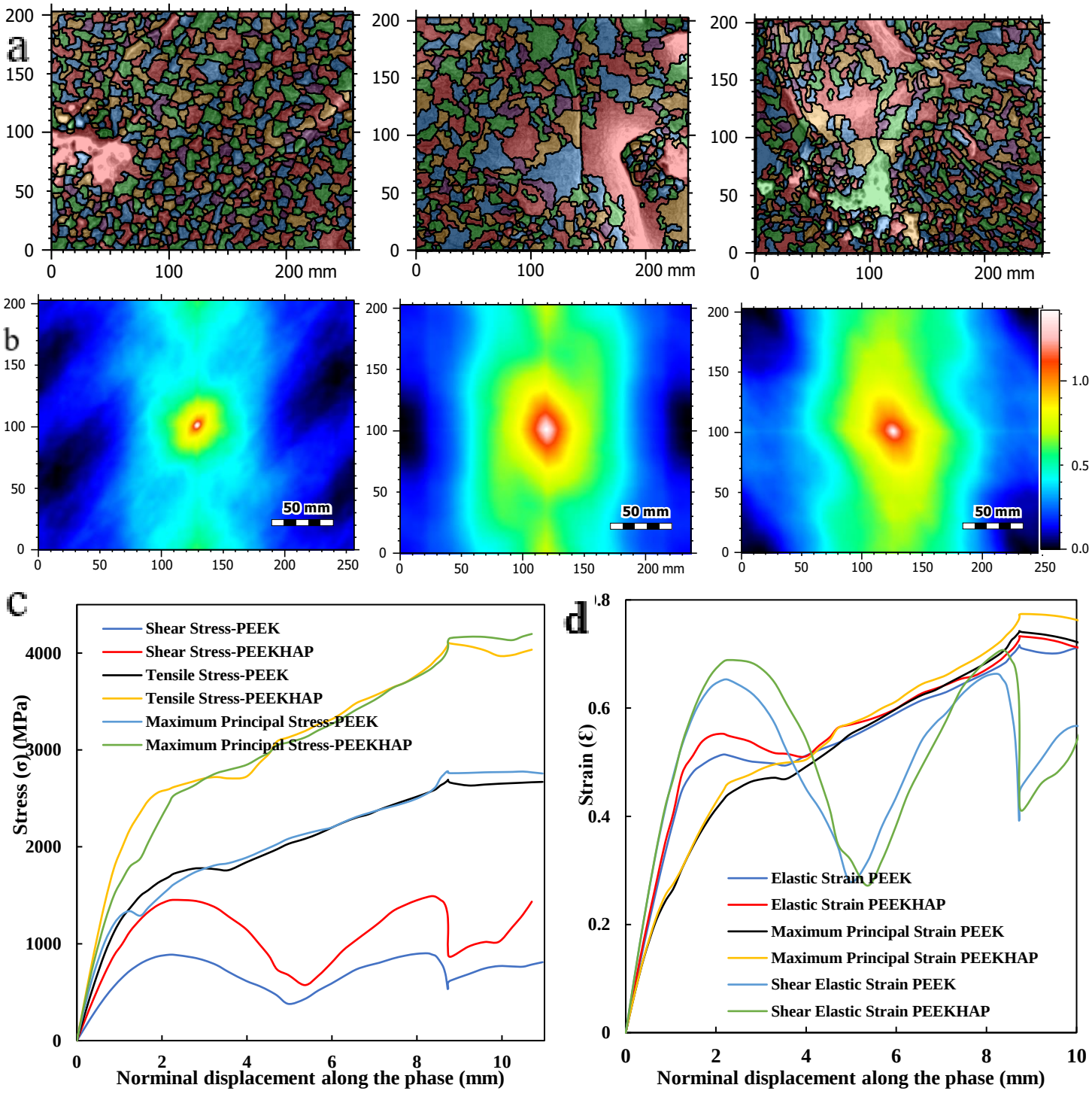

Fig. 13. Sample representation of (a) the living cell in the green of particles analysis in KL transform (b) surface autocorrelation of the sample structure, (c) mechanical stresses to average displacement along the face of test in representation and (d) strain representation for PEEK and PEEK-HAp during tensile test/experiment.

6. Conclusions

3D-printed PEEK-rGO-cHAp composite scaffolds have been additively manufactured through FMD technique and characterised for bone implants in tissue engineering applications. It was evident that the seven-

day composite exhibited better properties than other days, based on the results obtained from this study. The control, analysis and size of the grain can be determined by its porosity and mechanical end properties when applied to bond sintering powder. PEEK-cHAP performed better in strength than PEEK with a 2 to 3 MPa difference in their yield strengths from the stress analysis. PEEK-rich nanoparticles were dispersed in grains, and spherical nanoparticles grew in size after days of experimentation. Nanoparticle composite content of the gaussian (Ra) amplifying parameter in ISO standard decreased on the third day from 0.797 to 0.356 GL, with a tolerance limit of 0.751± 0.075 GL.

This study presents a formulation of a semi-stiff joint frame and combines that with a particular method of homogenisation. By analysing the Voxel models produced, we assess the effective structural parameters for the columns in the grid structures. This led to the effects of the AM process being investigated. Boards with more event groups have a higher typical ownership value. In addition, the construction angle affects the effective properties of the structure. To assess the effects of joint elasticity, parametric studies were performed, and study results showed that the curved grid is more sensitive than the controlled elongation lattices to common properties. Finally, we compare the projections of the proposed approach with the traditional homogenisation approach for validation. The evaluation showed that the proposed method could more accurately assess its mechanical properties. The predictions are more accurate as the proposed guidelines can capture the impact of AM processes and joint stiffening effects. Designers and engineers could use the proposed method for spine vertebrates that require additional weight or stiffness reduction, alleviating technical design problems.

Also, with the prepared PEEK-rGO-cHAp biocomposite scaffolds using FDM technology, it was observed that the addition of rGO and cHAP particles increased the biological activity of the PEEK to the PEEK matrix. Evaluating the tensile properties and modulus of elasticity of PEEK-cHAp compounds with different HAp levels ranging from 0 to 20% by weight, a cHAp of 15% by weight represented the ideal optimal percentage weight. In vitro DMEM culture medium tests showed PEEK-cHAp was better adhered to, proliferated, and active than pure PEEK. Lastly, the result obtained from the mixture of PEEK and cHAp compounds depicted excellent cell coagulation. However, the mechanical properties showed a small decrease because of the combination added. There is significant potential in PEEK-rGO-cHAp biocomposite scaffolds, as applied in bone implants/tissue or biomedical engineering.

References

[1] H. Yoshihara, Indirect decompression in spinal surgery, J. Clin. Neuros. 44 (2017) 63-68.

[2] C. Liao, Y. Li, S.C. Tjong, Polyetheretherketone and its composites for bone replacement and regeneration, Polymers 12 (2020) 1-48;

[3] *Bankole I. Oladapo, S. Abolfazl Zahedi, Sikiru O. Ismail, Francis T. Omigbodun, 3D printing of PEEK and its composite to increase biointerfaces as a biomedical material- A review, Colloids Surf. B: Biointerf., 203 (2021), Article 111726*

[4] G. Zhong, M. Vaezi, P. Liu, L. Pan, S. Yang, Characterisation approach on the 3D printing of bone tissue engineering scaffolds, Ceram. Inter. 43 (2017) 13860-13868.

[5] F.E. Bastan, M.A.U. Rehman, Y.Y. Avcu, E. Avcu, F. Ustel, A.R. Boccaccin, Electrophoretic co-deposition of PEEK-hydroxyapatite composite coatings for biomedical applications, Coll. Surf. B Biointerf. 169 (2018) 176-182.

[6] M. Tafaoli-Masoule, M. Shakeri, S.A. Zahedi, H. Seitz, M. Vaezi, 3D printing of PEEK-based medical devices Transactions on Additive Manufacturing Meets Medicine 1 (1) (2019).

[7] R.A. Lindtner, R. Schmid, T. Nydegger, M. Konschake, W. Schmoelz, Pedicle screw anchorage of carbon fiber-reinforced PEEK screws under cyclic loading. Eur. Spine J. 27 (2018) 1775–1784.

[8] C. Basgul, T. Yu, D.W. MacDonald, R. Siskey, M. Marcolongo, S.M. Kurtz, Structure–property relationships for 3D-printed peek intervertebral lumbar cages produced using fused filament fabrication, J. Mater. Res., 33 (2018) 2040-2051.

[9] *Bankole I. Oladapo, S. Abolfazl Zahedi, Sikiru O. Ismail, Mechanical performances of hip implant design and fabrication with PEEK composite, Polymer19 May 2021*

[10] S. Verma, N. Sharma, S. Kango, S. Sharma, Developments of PEEK (plyetheretherketone) as a biomedical material: A focused review, Eur. Polym. J. 147 (2021) 110295.

[11] S. Boriani, G. Tedesco, L. Ming, R. Ghermandi, M. Amichetti, P. Fossati, M. Krengli, L. Mavilla, A. Gasbarrini, Carbon-fiber-reinforced PEEK fixation system in the treatment of spine tumors: A preliminary report, Eur. Spine J. 27 (2018) 874-881.

[12] R. Ma, T. Tang, Current strategies to improve the bioactivity of PEEK, Int. J. Mol. Sci. 15 (2014) 5426–5445.

[13] O.K Bowoto, B.I. Oladapo, S.A. Zahedi, F.T. Omigbodun, O.P. Emenuvwe, Analytical modelling of in situ layer-wise defect detection in 3D-printed parts: additive manufacturing, Int. J. Adv. Manuf. Technol., 111 (7), 2311.

[14] Y. Liu, B. Rath, M. Tingart, J. Eschweiler, Role of implants surface modification in osseointegration: A systematic review, J. Biomed. Mater. Res. A 108 (2020) 470–484.

[15] F.B. Torstrick, A.S. Lin, D. Potter, D.L. Safranski, T.A. Sulchek, K. Gall, R.E. Guldberg, Porous PEEK improves the bone-implant interface compared to plasma-sprayed titanium coating on PEEK, Biomaterials 185 (2018) 106–116.

[16] F.B. Torstrick, D.L. Safranski, J.K. Burkus, J.L. Chappuis, C.S. Lee, R.E. Guldberg, K. Gall, K.E. Smith, Getting PEEK to stick to bone: The development of porous PEEK for interbody fusion devices, Tech. Orthop. 32 (2017) 158–166.

[17] Bankole I. Oladapo, S. Abolfazl Zahedi, Francis T. Omigbodun, A systematic review of polymer composite in biomedical engineering,European Polymer Journal23 May 2021.

[18] P. Johanson, R. Jimbo, Y. Kozai, T. Sakurai, P. Kjellin, F. Currie, A. Wennerberg, Nanosized hydroxyapatite coating on PEEK implants enhances early bone formation: A histological and three-dimensional investigation in rabbit bone, Materials 8 (2015) 3815–3830.

[19] D. Almasi, N. Iqbal, M. Sadeghi, I. Sudin, M.R.A. Kadir, T. Kamarul, Preparation methods for improving peek's bioactivity for orthopedic and dental application: A review, Int. J. Biomater. 12 (2016) 1-12.

[20] Bankole I.Oladapo, S. Abolfazl Zahedi, Vincent A.Balogun, Sikiru O.Ismail, Yarjan A.Samad, Overview of Additive Manufacturing Biopolymer Composites, Reference Module in Materials Science and Materials Engineering, 23 March 2021. https://doi.org/10.1016/B978-0-12-819724-0.00035-5.

[21] P. Johanson, R. Jimbo, Y. Naito, P. Kjellin, F. Currie, A. Wennerberg, Polyether ether ketone implants achieve increased bone fusion when coated with nano-sized hydroxyapatite: A histomorphometric study in rabbit bone, Int. J. Nanomed. 11 (2016) 1435–1442.

[22] S.M. Kurtz, J.N. Devine, Peek biomaterials in trauma, orthopedic, and spinal implants, Biomaterials 28 (2007) 4845-4869.

[23] B.I. Oladapo, S.O. Ismail, O.K. Bowoto, F.T. Omigbodun, M.A. Olawumi, Lattice design and 3D-printing of PEEK with Ca10 (OH)(PO4) 3 and in-vitro bio-composite for bone implant, Int. J. Biol. Macromol., 165, 50–62.

[24] C. Basgul, T. Yu, D.W. MacDonald, R. Siskey, M. Marcolongo, S.M. Kurtz, Structure-property relationships for 3D printed PEEK intervertebral lumbar cages produced using fused filament fabrication, J. Mater. Res. 33 (2018) 2040–2051.

[25] A. Wagner, E. Haag, A.K. Joerger, P. Jost, S.E. Combs, M. Wostrack, J. Gempt, B. Meyer, Comprehensive surgical treatment strategy for spinal metastases. Sci. Rep. 11 (2021) 1-11.

[26] B.I. Oladapo, A.O.M. Adeoye, M. Ismail, Analytical optimisation of a nanoparticle of microstructural fused deposition of resins for additive manufacturing, Compos. Part B Eng., 150 (2018), pp. 248-254

[27] K. Zhou, X. He, X. Tao, F. Pan, H. Yang, A biomechanical matched-pair comparison of two different locking plates for tibial diaphyseal comminuted fracture: Carbon fiber-reinforced poly-ether-ether-ketone (CF-PEEK) *versus* titanium plates, J. Orthop. Surg. Res. 15 (2020) 1-8.

[28] F-M. Chen, X. Liu, Advancing biomaterials of human origin for tissue engineering, Prog. Polym. Sci. 53 (2016) 86-168.

[29] *B.I. Oladapo, S.O. Ismail, T.D. Afolalu, D.B. Olawade, M. Zahedi, Review on 3D printing: Fight against COVID-19, Mater. Chem. Phys., 258, 123943.*

[30] D. Ho, T.H.T. Phan, R.J. Mobbs, R. Reddy, The use of radiolucent (carbon fibre-reinforced polymer) pedicle screw fixation for serial monitoring of clear cell meningioma: A case report, J. Surg. Case Rep. 12 (2020) 1-3.

[31] *B.I. Oladapo, S.A. Zahedi, A.O.M. Adeoye, 3D printing of bone scaffolds with hybrid biomaterials, Compos. Part B Eng., 158 (2019), pp. 428-436*

[32] F.B. Torstrick, N.T. Evans, H.Y. Stevens, K. Gall, R.E. Guldberg, Do surface porosity and pore size influence mechanical properties and cellular response to PEEK? Clin. Orthop. Relat. Res. 474 (2016) 2373–2383.

[33] S. Utzschneider, F. Becker, T.M. Grupp, B. Sievers, A. Paulus, O. Gottschalk, V. Jansson, Inflammatory response against different carbon fiber-reinforced PEEK wear particles compared with UHMWPE *in vivo*, Acta Biomater. 6 (2010) 4296–4304.

[34] *B.I. Oladapo, E.A. Oshin, A.M. Olawumi. Nanostructural computation of 4D printing carboxymethylcellulose (CMC) composite, Nano-Struct. Nano-Objects, 21, 100423.*

[35] A-K. Joerger, E. Shiban, S.M. Krieg, B. Meyer, Carbon-fiber reinforced PEEK instrumentation for spondylodiscitis: a single center experience on safety and efficacy, Sci. Rep. 11 (2021) 1-10.

[36] E. Shiban et al., analysis of bacterial adherence of clinical relevant staphylococcus species on carbon/PEEK composite vs standard titanium: Possible implications in spinal instrumentation for spondylodiscitis. Data presented as a poster at: EANS; Oktober 21–25, 2018; Brussels, Belgium (2018).

[37] *B.I. Oladapo, I.A. Daniyan, O.M. Ikumapayi, O.B. Malachi, I.O. Malachi, Microanalysis of hybrid characterisation of PLA/cHA polymer scaffolds for bone regeneration, Polym. Test., 83, 106341.*

[38] O. Uri, Y. Folman, G. Laufer, E. Behrbalk, A novel spine fixation system made entirely of carbon-fiber-reinforced PEEK composite: An *in vitro* mechanical evaluation, Adv. Orthoped. 2020 (2020) 1-7.

[39] M.F. Gornet, F.W. Chan, J.C. Coleman, B. Murrell, R.P. Nockels, B.A. Taylor, T.H. Lanman, J.A. Ochoa, Biomechanical assessment of a PEEK rod system for semi-rigid fixation of lumbar fusion constructs, J. Biomech. Eng. 133 (2011) 081009.

[40] *B.I. Oladapo, A.V. Adebiyi, E.I. Elemure, Microstructural 4D printing investigation of ultra-sonication biocomposite polymer, J. King Saud University-Eng. Sci.*

[41] R.D. Carpenter, B.S. Klosterhoff, F.B. Torstrick, K.T. Foley, J.K. Burkus, C.S.D. Lee, K. Gall, R.E. Guldberg, D.L. Safranski, Effect of porous orthopaedic implant material and structure on load sharing with simulated bone ingrowth: A finite element analysis comparing titanium and peek, J. Mech. Behav. Biomed. 80 (2018) 68-76.

[42] B. Berg-Johansen, S. Lovald, E. Altiok, S.M. Kurtz, Chapter 17 - Applications of polyetheretherketone in arthroscopy, S.M. Kurtz (Ed.), Peek Biomaterials Handbook (second edition), William Andrew Publishing (2019), 291-300.

[43] *B.I. Oladapo, O.I. Sikiru, Z. Mohsen, K. Affan, U. Hazrat, 3D printing and morphological characterisation of polymeric composite scaffolds, Eng. Struct., Article 110752.*

[44] C.S. Li, C. Vannabouathong, S. Sprague, M. Bhandari, The use of carbon-fiber-reinforced (CFR) PEEK material in orthopedic implants: A systematic review, Clinic Med. Insights Arth. Musculosk. Disord. 8 (2015) 33–45.

[45] G. Tedesco, A. Gasbarrini, S. Bandiera, R. Ghermandi, and S. Boriani, Composite PEEK/Carbon fiber implants can increase the effectiveness of radiotherapy in the management of spine tumors, J. Spine Surg. 3 (2017) 323–329.

[46] *O.P. Bodunde, O.M. Ikumapayi, E.T. Akinlabi, B.I. Oladapo, A.O.M. Adeoye, A futuristic insight into a "nano-doctor": A clinical review on medical diagnosis and devices using nanotechnology, Mater. Today: Proc.*

[47] A. Haleem, M. Javaid, Polyether ether ketone (peek) and its 3D-printed implants applications in medical field: An overview, Clin. Epidemiol. Global Health, 7 (2019) 571-577.

[48] J.F. Cao, Y. Lu, H.C. Chen, L.F. Zhang, C.D. Xiong, Preparation, properties and *in vitro* cellular response of multi-walled carbon nanotubes/bioactive glass/poly(etheretherketone) biocomposite for bone tissue engineering, Int. J. Polym. Mater. Polym. Biomater. 68 (2019) 433-441.

[49] V.A. Balogun, B.I. Oladapo, Electrical energy demand modeling of 3D printing technology for sustainable manufacture, Inter. J. Eng., 29 (2019), pp. 1-8

[50] H. Ma, A. Suonan, J. Zhou, Q. Yuan, L. Liu, X. Zhao, X. Lou, C. Yang, D. Li, Y-G. Zhang, PEEK (polyether-ether-ketone) and its composite materials in orthopedic implantation, Arab. J. Chem. 14 (2021) 102977.

[51] A. Nevelsky, E. Borzov, S. Daniel, R. Bar-Deroma, Perturbation effects of the carbon fiber-PEEK screws on radiotherapy dose distribution, J. Appl. Clin. Med. Phys. 18 (2017) 62–68.

[52] *Bankole, I. Oladapo, Abolfazl S. Zahedi, Improving bioactivity and strength of PEEK composite polymer for bone application, Mater. Chem. Phys. (2021), 10.1016/j.matchemphys.2021.124485*

[53] E.L. Steinberg, E. Rath, A. Shlaifer, O. Chechik, E. Maman, M. Salai, Carbon fiber reinforced PEEK Optima–a composite material biomechanical properties and wear/debris characteristics of CF-PEEK composites for orthopedic trauma implants, J. Mech. Behav. Biomed. Mater. 17 (2013) 221–228.

[54] B.I. Oladapo, S.A. Zahedi, Improving bioactivity and strength of PEEK composite polymer for bone application, Mater. Chem. Phys. 266 (2021) 124485.

[55] R.A.C.S. Brandão, W.C.D.S. Martins, A.A. Arantes Jr, S.N.S. Gusmão, G. Perrin, C. Barrey, Titanium *versus* polyetheretherketone implants for vertebral body replacement in the treatment of 77 thoracolumbar spinal fractures, Surg. Neurol. Int. 8 (2017) 1-7.

[56] G. Tedesco, A. Gasbarrini, S. Bandiera, R. Ghermandi, S. Boriani, Composite PEEK/carbon fiber implants can increase the effectiveness of radiotherapy in the management of spine tumors, J. Spine Surg. 3 (2017) 323–329.

[57] *B.I. Oladapo, S.A. Zahedi, F. Vahidnia, O.M. Ikumapayi, M.U. Farooq, Three-dimensional finite element analysis of a porcelain crowned tooth, Beni-Suef Univ. J. Basic Appl. Sci., 7 (2019), pp. 461-464*

[58] Y. Su, J. He, N. Jiang, H. Zhang, L. Wang, X. Liu, D. Li, Z. Yin, Additively-manufactured poly-ether-ether-ketone (PEEK) lattice scaffolds with uniform microporous architectures for enhanced cellular response and soft tissue adhesion, Mater. Des. 191 (2020) 108671.

[59] S. Boriani, V. Pipola, R. Cecchinato, R. Ghermandi, G. Tedesco, M.R. Fiore, F. Dionisi, A. Gasbarrini, Composite PEEK/carbon fiber rods in the treatment for bone tumors of the cervical spine: A case series, Eur. Spine J. 29 (2020) 3229–3236.

[60] J. Ma, B. Tang, Application of polyetheretherketone in the orthopaedic implants, Prog. Chem. 30 (2018) 1692-1700.

[61] S. Bess, J.E. Harris, A.W.L. Turner, V. LaFage, J.S. Smith, C.I. Shaffrey, F.J. Schwab, R.W. Haid Jr, The effect of posterior polyester tethers on the biomechanics of proximal junctional kyphosis: A finite element analysis, J. Neurosurg. Spine 26 (2017) 125–133.

[62] B.I. Oladapo, S.A. Zahedi, S.O. Ismail, F.T. Omigbodun, O.K. Bowoto, 3D printing of PEEK–cHAp scaffold for medical bone implant, Bio-Des. Manuf., 1–16.

[63] F. Ringel, Y.M. Ryang, J.S. Kirschke, B.S. Müller, J.J. Wilkens, J. Brodard, S.E. Combs, B. Meyer, Radiolucent carbon fiber-reinforced pedicle screws for treatment of spinal tumors: Advantages for radiation planning and follow-up imaging, World Neurosurg. 105 (2017) 294–301.

[64] Sang-in Park, David W. Rosen, Homogenisation of Mechanical Properties for Material Extrusion Periodic Lattice Structures Considering Joint Stiffening Effects, Journal of Mechanical Design. Received March 23, 2018;